

TEX-CUP: The University of Texas Challenge for Urban Positioning

Lakshay Narula, Daniel M. LaChapelle, Matthew J. Murrian, J. Michael Wooten, Todd E. Humphreys
Radionavigation Laboratory
The University of Texas at Austin
Austin, TX, USA

Elliot de Toldi, Guirec Morvant, Jean-Baptiste Lacambre
iXblue INC
Denver, CO, USA

Abstract—A public benchmark dataset collected in the dense urban center of the city of Austin, TX is introduced for evaluation of multi-sensor GNSS-based urban positioning. Existing public datasets on localization and/or odometry evaluation are based on sensors such as lidar, cameras, and radar. The role of GNSS in these datasets is typically limited to the generation of a reference trajectory in conjunction with a high-end inertial navigation system (INS). In contrast, the dataset introduced in this paper provides raw ADC output of wideband intermediate frequency (IF) GNSS data along with tightly synchronized raw measurements from inertial measurement units (IMUs) and a stereoscopic camera unit. This dataset will enable optimization of the full GNSS stack from signal tracking to state estimation, as well as sensor fusion with other automotive sensors. The dataset is available at <http://radionavlab.ae.utexas.edu> under Public Datasets. Efforts to collect and share similar datasets from a number of dense urban centers around the world are under way.

Index Terms—urban positioning; precise positioning; benchmark; dataset; sensor fusion.

I. INTRODUCTION

Development of automated ground vehicles (AGVs) has spurred research in lane-keeping assist systems, automated intersection management [1], tight-formation platooning, and cooperative sensing [2], [3], all of which demand accurate (e.g., 50-cm at 95%) ground vehicle positioning in an urban environment. But the majority of positioning techniques, and the associated performance benchmarks, developed thus far are based on lidar or cameras, which perform poorly in low-visibility conditions such as snowy whiteout, dense fog, or heavy rain. Adoption of AGVs in many parts of the world will require all-weather localization techniques.

Radio-wave-based sensing techniques such as radar and GNSS remain operable even in extreme weather conditions [4] because their longer-wavelength electromagnetic radiation penetrates snow, fog, and rain. Carrier-phase-differential GNSS (CDGNSS), also known as real time kinematic (RTK) GNSS, has been successfully applied for the past two decades as an all-weather decimeter-accurate localization technique in open-sky conditions. Similarly, inertial sensing techniques are also unaffected by weather conditions. A combination of low-cost inertial- and radio-based localization is a promising

direction towards precise all-weather urban positioning for AGVs.

While application of CDGNSS/RTK techniques for urban positioning has previously been limited due to expensive coupling with tactical grade IMUs [5], recent work has shown that 20-cm-accurate (95%) low-cost unaided CDGNSS positioning is possible at 87% availability with dual-frequency GPS and Galileo signals, even in the dense urban downtown of Austin, TX [6]. Similarly, [7] shows that unaided dual-frequency GPS-, BeiDou-, and GLONASS-based CDGNSS positioning can achieve decimeter-accurate (95%) positioning rate of 76.7% on a 1-hour drive along an urban route in Wuhan, China, and the availability can be further improved to 86.1% after integration with a MEMS IMU. Meanwhile, recent urban CDGNSS evaluation of commercial receivers in [8] indicates that no low-to-mid-range consumer CDGNSS solution offers greater than 35% decimeter-accurate solution availability in urban areas, despite a dense reference network and dual-frequency capability.

Similarly, until recently precise point positioning (PPP) algorithms required a long convergence time and as such were limited to surveying applications. With the proliferation of the number of GNSS satellites and better numerical models for atmospheric corrections [9], recent efforts have reported instantaneous convergence times for PPP in open sky or light urban conditions. The authors predict that efforts towards accuracy and availability of PPP in urban areas will be soon forthcoming.

The concern with development of GNSS-based precise positioning techniques as described above is that different algorithms may have been evaluated on datasets of different difficulties, even if the general environment may be described as urban. As an extreme example, consider the data collection route presented in Fig. 3. Over the entirety of the dataset, a Septentrio AsteRx4 RTK receiver used as a part of this data collection reports an integer-ambiguity-fixed RTK solution at 70.6% of all epochs. However, as is typical, the data collection routine involved ≈ 10 min stationary open-sky periods at the beginning and end of data collection. Excluding these periods brings down the fixed solution availability to 49.6% on the

arXiv:2005.00709v1 [cs.RO] 2 May 2020

remainder of the dataset. In fact, when restricted strictly to the dense urban southern portion of the test route, the availability of reported precise RTK solutions is only 21.3%. As such, it is at best challenging, and at worst misleading, to compare precise GNSS positioning algorithms on different datasets. Additionally, multipath properties of the GNSS antenna and phase stability of the sampling clock are other important factors that likely affect the performance analysis. In the opinion of the authors, the precise GNSS positioning community must converge on a shared and challenging dataset to evaluate their algorithms and thereby identify the critical components of a robust and accurate urban positioning engine.

As a precedent, similar benchmarks such as the KITTI dataset [10] for visual odometry and object segmentation, and the ImageNet dataset [11] for object instance recognition have served greatly towards the progress of their respective communities. The Oxford Robotcar Dataset [12] has been a similarly important benchmark dataset in the field of repeatable ground vehicle localization with lidars and cameras. However, none of the existing robotic localization datasets are focused on GNSS-based precise urban localization. The dataset being introduced in this paper addresses this gap for the GNSS research community.

The goal of the University of Texas Challenge for Urban Positioning is twofold: to enable the precise GNSS positioning community to evaluate and compare a variety of existing and upcoming techniques on a shared and challenging benchmark, and to save the time and effort required to assemble a high-quality data recording platform for urban positioning research.

II. SENSOR PLATFORM

The roving dataset is captured with an integrated perception platform named the University of Texas *Sensorium*, shown in Figs. 1 and 2, equipped with the following sensors:

- 2× Antcom G8Ant-3A4TNB1 high performance GNSS patch antennas (NGS code: ACCG8ANT_3A4TB1). Triple frequency L1/L2/L5; 40 dB low-noise amplifier.
- 1× RadioLynx GNSS RF front end. Dual frequency L1/L2; 5 Msps bandwidth on both channels; support for two GNSS antennas; developed in-house; provided with Bliley LP-62 low-power 10 MHz OCXO external reference.
- 1× NTLab B1065U1-12-X configurable RF front end. Configured to capture L1/L2/L5 signals from one GNSS antenna with a wide bandwidth of 53 Msps; provided with Bliley LP-62 low-power 10 MHz OCXO external reference.
- 1× u-blox EVK-M8T. Single-frequency (L1) multi-constellation mass-market receiver.
- 1× Bosch BMX055 9-axis IMU. Low-cost MEMS device; smartphone-grade IMU noise characteristics; 150 Hz output rate.
- 1× LORD MicroStrain 3DM-GX5-25 AHRS. High-performance MEMS device; industrial-grade IMU noise characteristics; 100 Hz output rate.

- 2× Basler acA2040-35gm cameras. 2048 × 1536 resolution; monochromatic; Sony IMX265 CMOS sensor; global shutter; hardware triggered at 10 fps; ≈50 cm baseline; Kowa LMVZ4411 lenses.
- 1× Delphi ESR 2.5 (24VDC) L2C0051TR electronically scanning radar. Simultaneous mid- and long-range measurement modes; mid-range 60 m, 90° field-of-view; long-range 174 m, 20° field-of-view; 20 Hz scan rate.
- 2× Delphi SRR2 single beam monopulse radars. Range 80 m; field-of-view 150°; 20 Hz scan rate. When mounted as shown in Figs. 1 and 2, the three radars provide 210° of coverage around the vehicle.
- 1× Taoglas 4G LTE MIMO antenna. Provides connectivity to the network for CDGNSS corrections.

For the purposes of this evaluation dataset, the Sensorium is equipped with an iXblue ATLANS-C: a high-performance RTK-GNSS coupled fiber-optic gyroscope (FOG) INS (not shown in Figs. 1 and 2). The Septentrio AsteRx4 RTK receiver inside the ATLANS-C is attached to one of the two GNSS antennas, and tracks most constellations on all three GNSS frequencies. The post-processed fused RTK-INS position solution obtained from the ATLANS-C is taken to be the ground truth trajectory.

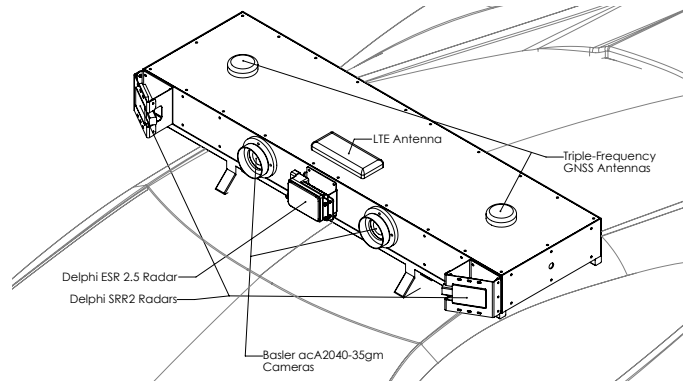


Fig. 1. The University of Texas Sensorium is a platform for automated and connected vehicle perception research. The Sensorium features two L1/L2/L5 GNSS antennas, wideband GNSS RF front ends, smartphone- and industrial-grade MEMS IMUs, stereoscopic cameras, automotive radars, and LTE connectivity.

The Sensorium houses a rugged Nuvis N5306RT computer with a modest desktop-level configuration. The computer runs Ubuntu Linux and logs data from all sensors and devices. Most data logging processes are developed in-house for precise synchronization between sensor data. Details on sensor synchronization are provided in Sec. IV-C.

To enable CDGNSS-based positioning, the dataset also includes GNSS data logged from a nearby reference antenna with a clear view of the sky. The reference antenna is a geodetic-grade Trimble Zephyr II (NGS code: TRM57971.00). For consistency with the rover, raw IF reference data is logged with identical RadioLynx and NTLab RF front ends. For completeness, RINEX-format reference data from an identical Septentrio AsteRx4 receiver is also logged. The rover platform

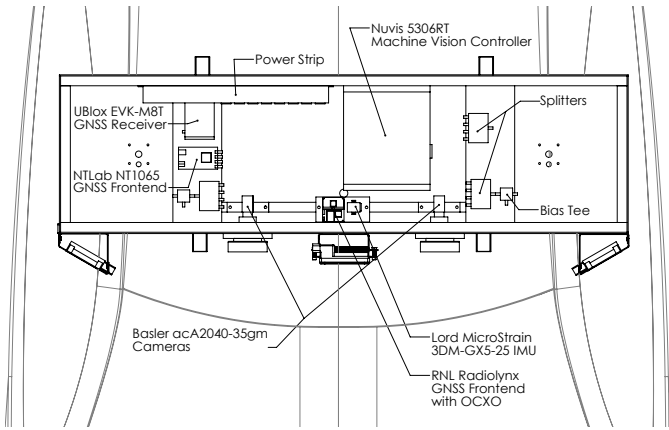


Fig. 2. Inside view of the University of Texas Sensorium, showing the internal organization of a desktop-class computer, IMUs, two GNSS RF front ends, and a stereoscopic camera setup.

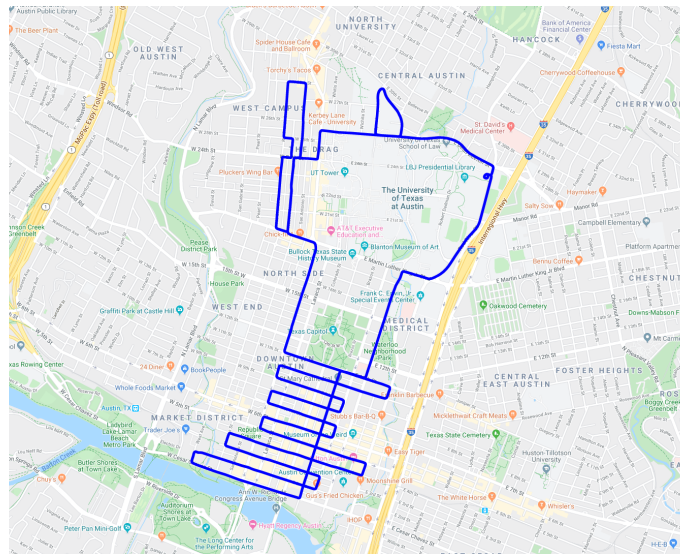


Fig. 3. Test route through The University of Texas west campus and Austin downtown. These areas are the most challenging for precise GNSS-based positioning. The route was driven once on a weekday and again on the weekend to evaluate robustness of mapping-based methods to changes in traffic and parking patterns.

is always within 4 km of the reference antenna, representing ideal CDGNSS conditions.

III. DATA COLLECTION

The test route, depicted in Fig. 3, runs the gamut of light-to-dense urban conditions, from open-sky to narrow streets with overhanging trees to the high-rise urban city center.

The data capture begins and ends with a stationary interval of several minutes in open sky conditions to allow confident bookending for the ground truth system. The first part of the trajectory runs through the semi-urban conditions north of the University of Texas campus, passing under two pedestrian bridges. The second part of the trajectory passes through an area with narrow streets lined by tall residential apartment buildings and dense foliage. The rest of the test route combs through the dense urban center of the city of Austin, TX, driving through every east-west street in the city downtown.

The number of signals tracked by a receiver is a good indicator of the level of difficulty posed by the dataset. Fig. 4 shows two extremes of this metric by comparing the low-cost mass-market u-blox M8T and the high-performance all-in-view Septentrio AsteRx4. As mentioned before, the u-blox M8T is a single frequency receiver, and is only able to track GPS and GLONASS signals in the presented dataset. The number of tracked signals during the 30 min challenging downtown portion of the dataset is under 15 for the M8T, making it unlikely to produce reliable CDGNSS position estimates [6]. At the other end of the performance spectrum, the AsteRx4 receiver is a state-of-the-art all-in-view receiver, tracking all constellations in all GNSS bands. For this receiver, the number of tracked signals is above 20 for most of the challenging portion of the dataset.

Fig. 5 shows Google Street View imagery from the driven route for a qualitative assessment of the dataset difficulty. A KML file with the full route is provided along with the dataset for easy visualization of the urban conditions.

The trajectory shown in Fig. 3 is driven twice, once on Thursday, May 9, 2019, and again on Sunday, May 12,

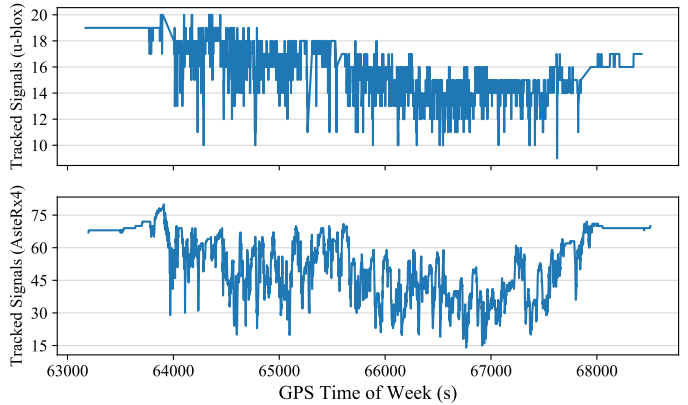


Fig. 4. A comparison of the number of tracked signals over the duration of the dataset for the u-blox M8T receiver (top) and the Septentrio AsteRx4 receiver (bottom). The u-blox M8T is an L1-only receiver tracking GPS and GLONASS signals. The Septentrio AsteRx4 is a triple-frequency all-in-view receiver.

2019. The repeated trajectory enables use of mapping-based techniques and their evaluation with sufficient variation in traffic and parking patterns between a weekday and a weekend.

A. Data Formats

This section describes the formats of different sensor data made available as part of this dataset. The description is organized by the different devices generating the data.

1) *RadioLynx Front End*: The RadioLynx RF front end generates two-bit-quantized samples from two antennas at the rover and a single antenna at the reference station, capturing 4.2MHz bandwidth at both L1 and L2 bands around the GPS frequencies. The raw IF data from the three antennas is made available in a binary format documented along with

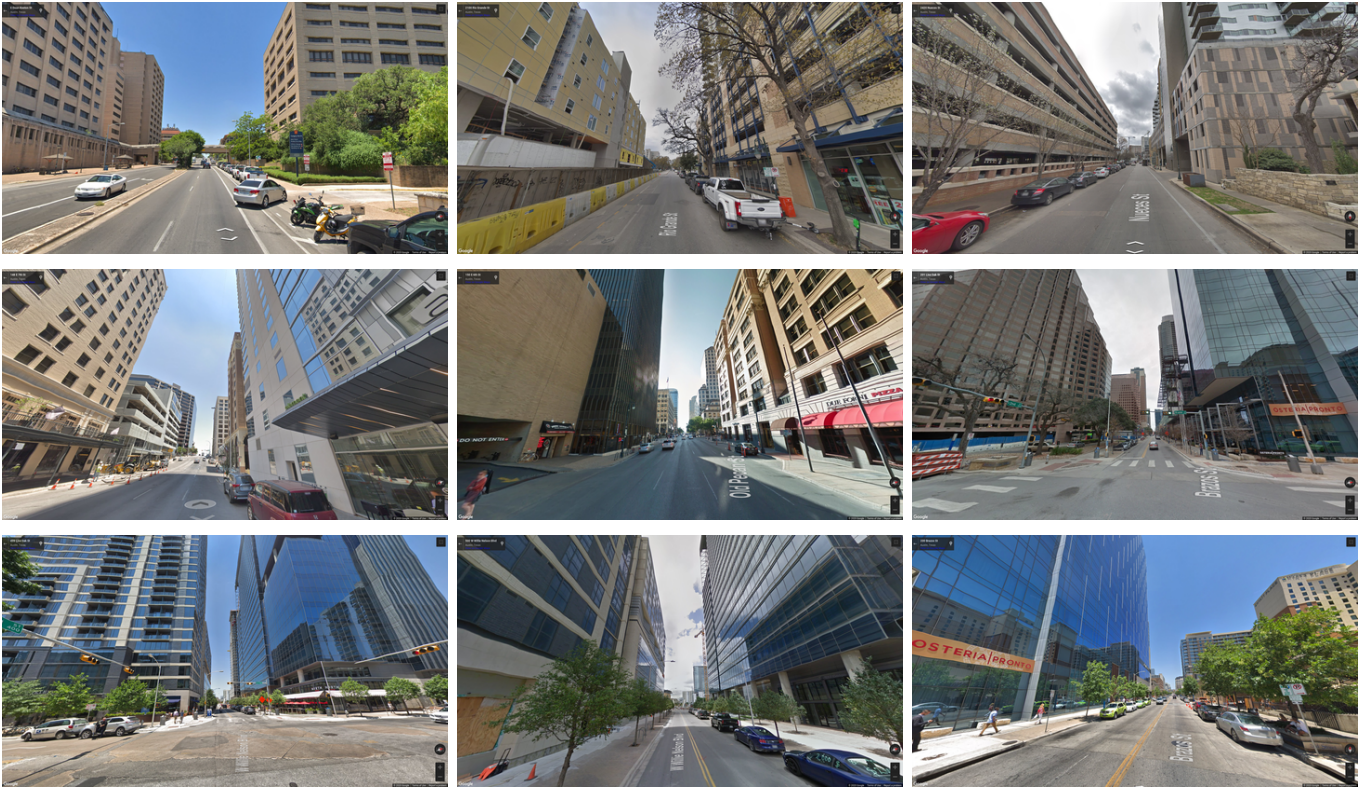


Fig. 5. Google Street View imagery of a few challenging scenarios encountered in the dataset.

the dataset, including the required IF parameters. Raw IF data enable development of new signal tracking strategies for urban precise positioning, and allow high-sensitivity receivers to track weak signals that may not have been tracked by the receivers in the recording platform. Raw IF samples from the reference antenna can be used for data bit wipeoff [6, Sec. III-D], if desired.

The dataset also provides tracked pseudorange and carrier-phase observables generated by the GRID software-defined receiver [6] operating on the RadioLynx raw IF samples for both rover antennas and the reference antenna. At the time of writing, the GRID receiver tracks GPS, Galileo, and SBAS signals. The observables are provided in the RINEX format.

2) *NtLab Front End*: The NtLab RF front end produces two-bit-quantized samples from one of the two rover antennas and the antenna at the reference station. With a sample rate of 79.5 MHz, the NtLab front end captures signals at L1, L2, and L5 frequencies with a wide bandwidth. The raw IF data from both the rover and reference antennas are made available at this time, tracked observables in RINEX format will be made available soon.

3) *Septentrio AsteRx4*: The Septentrio AsteRx4 receiver housed inside iXblue ATLANS-C produces observables for GPS, Galileo, GLONASS, BeiDou, and SBAS at all three GNSS frequencies. All these observables are made available in RINEX format.

4) *u-blox M8T*: The NMEA output from the u-blox M8T receiver is provided with the dataset for comparison to a

competitive mass-market receiver.

5) *Stereo Cameras*: Timestamped stereo images from the two Basler cameras are made available in HDF5 format. As detailed later in Sec. IV-C, camera images are timestamped by the Sensorium computer when the image is received over Ethernet. The dataset also provides the exposure time for individual images if it may be desirable to account for its variation.

Accurate intrinsic and extrinsic calibration of cameras is important for camera-based positioning. This dataset provides an HDF5 archive of stereo and monocular calibration images captured with the Sensorium before the data capture, along with measurements of the calibration patterns. These archives may be used to obtain both intrinsic and extrinsic calibration parameters as required, e.g., using the Kalibr calibration toolbox [13].

6) *Bosch IMU*: To evaluate the benefit of low-cost inertial aiding in urban areas, the dataset includes timestamped specific force, angular rate, and temperature measurements from the Bosch BMX055 IMU in CSV format. This IMU is built-in to the RadioLynx board, and has been set up such that the IMU data timestamps can be traced back to the GNSS RF sampling clock. This enables highly accurate correspondence between the IMU timestamps and GPS time.

7) *LORD MicroStrain IMU*: Timestamped specific force and angular rate measurements from the high-performance LORD MicroStrain MEMS IMU are made available in CSV format. The LORD IMU accepts a PPS (pulse per second)

signal generated by the u-blox receiver to synchronize to GPS time. LORD IMU measurements are internally compensated for temperature variation.

8) *ATLANS-C IMU*: The dataset includes specific force and angular rate measurements from the highly stable accelerometers and FOGs housed in the iXblue ATLANS-C. These data are only made available from the May 9, 2019 data collection session. The ATLANS-C data from May 12, 2019 data are held back for performance evaluation.

9) *Ground Truth Trajectory*: A trustworthy ground truth trajectory against which to compare the reported trajectory of a system under test is indispensable for urban positioning evaluation. Post-processing software provided by iXblue generates a forward-backward smoothed position and orientation solution with fusion of AsteRx4 RTK solutions and inertial measurements. The post-processed solution is accurate to better than 20 cm throughout the dataset, and may be considered as the ground truth trajectory. As with the ATLANS-C IMU measurements, the ground truth trajectory is only made available from the May 9, 2019 session. The ground truth trajectory from May 12, 2019 is withheld for evaluation of community solutions. The authors may advertise the performance of community submissions on the dataset webpage with consent from the developer.

B. Interface with Receivers

The dataset is easiest to interface to with a software-defined receiver, since these receivers typically accept a stream of digitized IF samples as the input. For receivers that only accept RF input, it may be possible to replay the provided raw IF samples after upconversion to RF with use of a GNSS replay/playback system similar to LabSat 3 Wideband [14].

C. Planned Worldwide Extension

In partnership with iXblue, TEX-CUP is currently being extended to include raw GNSS IF and IMU data from various worldwide dense urban centers. These future data captures will use a simplified version of the Sensorium rover platform, including the same NTLab and RadioLynx front ends, a newer u-blox receiver (ZED-F9P), as well as the Septentrio AsteRx4 and ATLANS A7 (upgraded version of the ATLANS-C) or ATLANS A9 (best in class) INS for the ground truth trajectory. Raw IMU data from the Bosch BMX055 and ATLANS will also be included.

Urban centers currently under consideration for future data collection include Denver, CO, Boston, MA, and San Diego, CA in the US, and Paris, Amsterdam, Singapore, and Beijing internationally.

IV. SENSOR CALIBRATION & SYNCHRONIZATION

Accurate calibration and synchronization of all sensors is critical for any localization dataset. The performance of GNSS/INS, odometry, and SLAM techniques strongly depends on the accuracy of sensor calibration and synchronization.

A. Intrinsic Calibration

Intrinsic sensor calibration is necessary for cameras and IMUs, while antenna and front-end calibration may be beneficial in high-accuracy and high-availability GNSS applications.

1) *Cameras*: Intrinsic camera calibration may be performed by capturing images of a known calibration pattern at different scales and orientations. The dataset includes such a capture for the Sensorium cameras. These images may be used with a tool such as Kalibr [13] to obtain intrinsic camera parameters including focal length, principal point, lens distortion, etc. It must be noted that platform vibrations during data collection can lead to small variations in the intrinsic calibration parameters. It is most desirable to continuously track the calibration parameters in real time in combination with CDGNSS and/or IMUs.

2) *IMUs*: The dataset provides a 24 h long stationary capture of IMU measurements from the Bosch and LORD IMUs to enable calibration of IMU noise and bias stability parameters. In addition to noise and bias stability, IMU intrinsic calibration involves estimation of accelerometer and gyroscope biases and scale factors. Unfortunately, *a priori* intrinsic calibration is typically not feasible due to variable turn-on-to-turn-on bias properties of the IMUs. It is thus common to track the IMU bias and scale factor parameters in combination with GNSS and/or vision-based positioning [15].

3) *GNSS Antennas*: Intrinsic calibration of the Sensorium's two GNSS antennas amounts to developing a model for antenna phase center variations (PCVs) as a function of the direction of arrival of an incoming signal. Such a calibration can be obtained at the carrier phase level either relative to a reference antenna, as in [16], or in absolute terms, as in [17]. The U.S. National Geodetic Survey (NGS) offers absolute calibration files for a wide variety of antenna models, including for the type of antenna on the Sensorium (NGS code: ACCG8ANT_3A4TB1) and at the reference station (NGS code: TRM57971.00)¹. Users of the TEX-CUP data will tend to see improved CDGNSS availability and accuracy when these calibrations are applied.

PCV models such as offered by the NGS cannot, however, compensate for local effects: The Sensorium's antennas are mounted on a broad aluminum backplane that affects the antennas' PCV behavior in a way not captured by the NGS model. To obtain a more accurate PCV model for use with the TEX-CUP data set, a relative calibration was performed between each of the Sensorium's antennas *in situ* and the TEX-CUP reference antenna. GNSS phase and pseudorange observables were collected over a two-day period and a PCV modeling procedure like the one presented in [16] was performed, except that the model was based on double-rather than single-difference carrier phase measurements. Let z represent the zenith angle (angular departure from the antenna boresight), and a represent the azimuth angle of an incoming signal, both in radians. Then the additional carrier phase

¹See <https://www.ngs.noaa.gov/ANTCAL/index.xhtml>

length, in meters, for a signal arriving from direction (z, a) is modeled as

$$d(z, a) = \left(\sum_{i=1}^n g_i z^i \right) \left[1 + \sum_{j=1}^m g_{cj} \cos(ja) + g_{sj} \sin(ja) \right]$$

Azimuthal coefficients g_{cj} and g_{sj} , and elevation coefficients g_i , are obtained via a nonlinear least squares fitting procedure. Separate sets of coefficients may be obtained for each of the antennas' three receiving frequencies.

The azimuthal coefficients were found to be too small to be estimated reliably from the two-day data set, but the elevation coefficients were significant and are available on the TEX-CUP website for both starboard and port Sensorium antennas at both L1 and L2. Application of these coefficients reduces the standard deviation of L1 and L2 undifferenced carrier phase residuals by 11% and 15%, respectively, in the 2-day PCV calibration data set. Coefficients for the L5 frequency will be posted to the TEX-CUP website in the future.

4) *GNSS Code Phase Biases*: Differential code phase biases arise in GNSS receivers due to dissimilar frequency paths and dissimilar autocorrelation functions [18]. Thus, a bias may arise between GPS L1 C/A and GPS L2C code phase measurements even though the signals have similar autocorrelation properties, and between GPS L1 C/A and Galileo E1 measurements even though the signals have identical center frequencies. A similar bias exists at each GNSS satellite.

Monthly estimates of the satellite-side biases are available from the Center for Orbit Determination in Europe (CODE)². Once these are applied, it is straightforward to estimate the receiver-side biases relative to a reference signal, usually taken to be GPS L1 C/A. During the 10-minute stationary periods that bookend each TEX-CUP data interval, a GPS L1 C/A-only CDGNSS solution can be obtained for each of the Sensorium's antennas. Due to the short Sensorium-to-reference baseline (less than 1 km during these stationary segments), and to averaging over the 10-minute period, this solution is accurate to better than 1 cm. Once obtained, this solution can be used as a truth constraint on the antennas' location. Next, a high-accuracy ionospheric model such as the final TEC grid of the International GNSS Service [19], [20] is applied to compensate for ionospheric delays in code phase. Finally, the receiver's differential code phase biases are estimated by averaging pseudorange residuals for each signal when the antennas are constrained to their known location.

B. Extrinsic Calibration

Extrinsic calibration involves estimation of the relative positions and orientations of different sensors involved in sensor fusion. Fig. 6 shows the coordinate frames involved in the dataset, and lever arm measurements between these frames. The sensor mounts are machined to maintain 90° rotations between the sensors. However, it is possible that the tolerances involved in this process may not be sufficiently accurate for high-precision positioning. Accordingly, the provided extrinsic

parameters should be considered as initial estimates to an online calibration procedure.

Note that the camera calibration data captures mentioned above may be used to estimate the extrinsic parameters between the two cameras. As noted before, these parameters have been observed to vary due to platform vibrations and must ideally be tracked in real time.

C. Synchronization

Sensorium IMU and camera measurements are synchronized to GPS time. The Bosch IMU is built-in to the RadioLynx board, enabling direct synchronization to the RadioLynx sample clock, and by extension to GPS time. The LORD MicroStrain IMU accepts a PPS signal from the u-blox receiver and GPS week and whole seconds over USB from the software-defined GNSS receiver running on the Sensorium computer. The synchronization to GPS time is handled internally by the LORD IMU. Similarly, the ATLANS-C IMU measurements and fused ground truth trajectory are internally synchronized to GPS time (but reported in UTC time).

The Sensorium computer clock is itself synchronized to GPS time to within less than a millisecond by pointing the computer's NTP client to the GPS time reported by the software receiver running on the machine. This enables the Sensorium computer to timestamp any sensor data with sub-millisecond accuracy to GPS time.

The Basler cameras in the Sensorium accept an external hardware trigger to capture images. The trigger is generated by the RadioLynx board at ≈ 10 Hz in synchronization with the sampling clock ticks. As a result, the trigger provided to the cameras can be traced back to the GNSS sample recorded by the RadioLynx front end. There are two major sources of delay that may be taken in to account when processing camera images. First, after receiving the hardware trigger, the cameras expose the sensor for a variable amount of time, depending on the lighting conditions. Fortunately, the Basler API provides access to the exposure time for each image. The provided dataset annotates each individual image with the exposure time reported by the camera. Second, the images are timestamped by the Sensorium computer when these images are received over the local Ethernet connection. The data transfer time from the camera to the computer is typically very stable since no other devices are on the network, and may be estimated as a constant parameter in real time, if necessary.

V. SUMMARY & FUTURE EXTENSIONS

A GNSS-based precise positioning benchmark dataset collected in the dense urban center of Austin, TX has been introduced. With provision of raw wideband IF GNSS data along with tightly synchronized raw measurements from multiple IMUs and a stereoscopic camera unit, the authors hope that the precise GNSS positioning community will benefit from testing their techniques on a challenging public dataset. In the near future, the authors hope to offer a benchmarking service similar to the KITTI benchmark suite [10], providing the opportunity for researchers to publicly compare precise

²See <http://ftp.aiub.unibe.ch/CODE/>

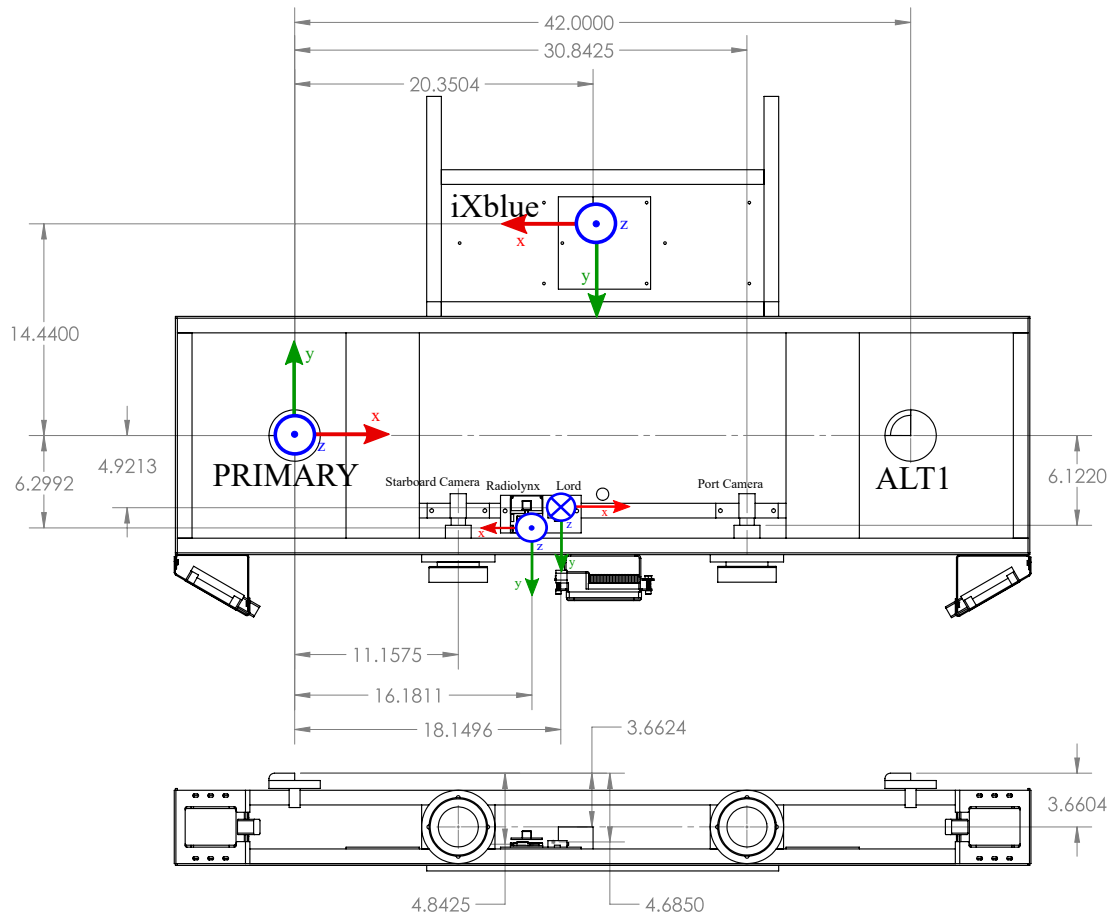


Fig. 6. Computer drawing showing the position and orientation of the sensors used in this dataset from a top view (top panel) and a front view (bottom panel). Measurements are provided in inches. Note that the indicated coordinate axes are assumed to be perfect 90° rotations from each other. The \odot symbol denotes an out-of-page axis, while the \otimes symbol denotes an in-to-page axis.

urban positioning methods. The dataset will soon be extended to include wideband GNSS IF data collected in several other urban centers around the world.

REFERENCES

- [1] D. Fajardo, T.-C. Au, S. Waller, P. Stone, and D. Yang, "Automated intersection control: Performance of future innovation versus current traffic signal control," *Transportation Research Record: Journal of the Transportation Research Board*, no. 2259, pp. 223–232, 2011.
- [2] J. Choi, V. Va, N. Gonzalez-Prelcic, R. Daniels, C. R. Bhat, and R. W. Heath, "Millimeter-wave vehicular communication to support massive automotive sensing," *IEEE Communications Magazine*, vol. 54, no. 12, pp. 160–167, December 2016.
- [3] D. LaChapelle, T. E. Humphreys, L. Narula, P. A. Iannucci, and E. Moradi-Pari, "Automotive collision risk estimation under cooperative sensing," in *Proceedings of the IEEE International Conference on Acoustics, Speech, and Signal Processing*, Barcelona, Spain, 2020.
- [4] K. S. Yen, C. Shankwitz, B. Newstrom, T. A. Lasky, and B. Ravani, "Evaluation of the University of Minnesota GPS Snowplow Driver Assistance Program," Tech. Rep., 2015.
- [5] M. Petovello, M. Cannon, and G. Lachapelle, "Benefits of using a tactical-grade IMU for high-accuracy positioning," *Navigation, Journal of the Institute of Navigation*, vol. 51, no. 1, pp. 1–12, 2004.
- [6] T. E. Humphreys, L. Narula, and M. J. Murrian, "Deep urban unaided precise GNSS vehicle positioning," *IEEE Intelligent Transportation Systems Magazine*, 2020, to be published.
- [7] T. Li, H. Zhang, Z. Gao, Q. Chen, and X. Niu, "High-accuracy positioning in urban environments using single-frequency multi-GNSS RTK/MEMS-IMU integration," *Remote Sensing*, vol. 10, no. 2, p. 205, 2018.
- [8] J. Jackson, B. Davis, and D. Gebre-Egziabher, "An assessment of low-cost RTK GNSS receivers," in *Proceedings of the IEEE/ION PLANS Meeting*, Monterey, CA, 2018.
- [9] S. Banville, P. Collins, W. Zhang, and R. B. Langley, "Global and regional ionospheric corrections for faster PPP convergence," *Navigation*, vol. 61, no. 2, pp. 115–124, 2014.
- [10] A. Geiger, P. Lenz, C. Stiller, and R. Urtasun, "Vision meets robotics: The KITTI dataset," *International Journal of Robotics Research (IJRR)*, 2013.
- [11] J. Deng, W. Dong, R. Socher, L.-J. Li, K. Li, and L. Fei-Fei, "ImageNet: A large-scale hierarchical image database," in *2009 IEEE Conference on Computer Vision and Pattern Recognition*. IEEE, 2009, pp. 248–255.
- [12] W. Maddern, G. Pascoe, C. Linegar, and P. Newman, "1 Year, 1000km: The Oxford RobotCar Dataset," *The International Journal of Robotics Research (IJRR)*, vol. 36, no. 1, pp. 3–15, 2017. [Online]. Available: <http://dx.doi.org/10.1177/0278364916679498>
- [13] P. Furgale, J. Rehder, and R. Siegwart, "Unified temporal and spatial calibration for multi-sensor systems," in *2013 IEEE/RSJ International Conference on Intelligent Robots and Systems*. IEEE, 2013, pp. 1280–1286.
- [14] LabSat, "LabSat 3 Wideband," Feb. 2019, <https://www.labsat.co.uk/index.php/en/products/labsat-3-wideband>.
- [15] M. Kok, J. D. Hol, and T. B. Schön, "Using inertial sensors for position and orientation estimation," *arXiv preprint arXiv:1704.06053*, 2017.
- [16] G. L. Mader, "GPS antenna calibration at the National Geodetic Survey,"

GPS solutions, vol. 3, no. 1, pp. 50–58, 1999.

- [17] A. Bilich and G. L. Mader, “Gnss absolute antenna calibration at the national geodetic survey,” in *Proceedings of the 2010 ION GNSS Conference*, 2010.
- [18] O. Montenbruck, A. Hauschild, and P. Steigenberger, “Differential code bias estimation using multi-gnss observations and global ionosphere maps,” *Navigation: Journal of the Institute of Navigation*, vol. 61, no. 3, pp. 191–201, 2014.
- [19] M. Hernández-Pajares, J. M. Juan, J. Sanz, R. Orus, A. Garcia-Rigo, J. Feltens, A. Komjathy, S. C. Schaer, and A. Krankowski, “The igs vtec maps: a reliable source of ionospheric information since 1998,” *Journal of Geodesy*, vol. 83, no. 3, pp. 263–275, Mar 2009. [Online]. Available: <https://doi.org/10.1007/s00190-008-0266-1>
- [20] L. Narula, J. M. Wooten, M. J. Murrian, D. M. LaChapelle, and T. E. Humphreys, “Accurate collaborative globally-referenced digital mapping with standard GNSS,” *Sensors*, vol. 18, no. 8, 2018. [Online]. Available: <http://www.mdpi.com/1424-8220/18/8/2452>